Electric modulation of conduction in MAPbBr3 single crystals

Shanming Ke
Nanchang University
Shangyu Luo
Nanchang University
Jinhui Gong
Nanchang University
Liwen Qiu
Nanchang University
Renhong Liang
Nanchang University
Yangbo Zhou
Nanchang University
Bingcheng Luo
NPU: Northwestern Polytechnical University
Baochang Cheng
Nanchang University
Li Wang
Nanchang University
longlong shu (llshu@ncu.edu.cn)
Nanchang University https://orcid.org/0000-0002-7121-1652

Research Article

Keywords: resistive switching, rectifying behavior, hybrid organic-inorganic perovskites, p-n structure

Posted Date: December 4th, 2020

DOI: https://doi.org/10.21203/rs.3.rs-67676/v2

Electric modulation of conduction in $MAPbBr_3$ single crystals

Shanming Ke,[†] *Shangyu Luo,*[†] *Jinhui Gong,*[†] *Liwen Qiu,*[†] *Renhong Liang,*[†] *Yangbo Zhou,*[†] *Bingcheng Luo,*[‡] *Baochang Cheng,*[†] *Li Wang,*[*,†] *Longlong Shu*[*,†]

[†] School of Materials Science and Engineering, Nanchang University, Nanchang 330031, People's Republic of China

[‡] State Key Laboratory of Solidification Processing, Northwestern Polytechnical University, Xi'an 710072, People's Republic of China

■ ABSTRACT

The resistive switching (RS) mechanism of hybrid organic-inorganic perovskites is an open question until now. Here, a switchable diode-like RS behavior in $MAPbBr_3$ single crystals using Au (or Pt) symmetric electrodes is reported. Both the high resistance state (HRS) and low resistance state (LRS) are electrode-area dependent and light responsive. We propose an electric-field-driven inner p-n junction accompanied by a trap-controlled SCLC conduction mechanism to explain this switchable diode-like RS behavior in $MAPbBr_3$ single crystals.

Keywords: resistive switching, rectifying behavior, hybrid organic-inorganic perovskites, p-n structure

■ INTRODUCTION

Currently, hybrid organic-inorganic perovskites (HOIPs) have been dynamically investigated for the potential applications in solar cells,[1] light-emitting diodes,[2,3] photodetectors,[2,3] lasers[4] and transistors.[5] For perovskite solar cells, a large electrical hysteresis in current-voltage (*I-V*) curves has been frequently reported, which is generally attributed to ferroelectricity,[6] charge trapping,[7] or ion migration.[8] Although the large hysteresis needs to be eliminated in optoelectric devices, this phenomenon inspired the observation of resistive switching (RS) behavior in hybrid perovskite films,[9-16] which is exploited for multilevel data storage.

RS phenomena have attracted a very large interest in the last years. Generally, the RS devices with a capacitor-like structure could be switched by an external bias to two different resistance states, a high resistance state (HRS) and a low resistance state (LRS). A wide variety of inorganic, organic and organic-inorganic hybrid materials have been found to display resistive switching features thus far.[17,18] Yoo *et al.*[9] reported the RS behavior for the first time in $MAPbI_{3-x}Cl_x$ (MA is shorted for $CH_3NH_3^+$) perovskite films, and proposed a mechanism based on the trap-controlled space-charge-limited conduction (SCLC). Recently, interface-type RS was observed in $MAPbBr_3$ thick films (1 μm) by Guan *et al.*[10] They proposed that the switching mechanism could be due to the migration of MA vacancies and the modification of the interfacial Schottky barrier. The filamentary-type RS has also been observed in several other works on $MAPbI_3$-based thin films (100 - 400 nm), where the conducting filaments were attributed to the migration of anions defects[11-13] or Ag ions from the redox reactions of Ag electrode.[14,15] Moreover, the RS behavior of HOIPs could be strongly influenced by illumination. Chai *et al.*[16] found that the set voltage could be greatly lowered under light illumination in

$MAPbI_3$-based RS devices. However, in a previous work,[19] we found no meaningful RS behavior in an individual $MAPbI_3$ nanowire unless under light illumination. These results clearly indicate that there remain many open questions regarding RS phenomena and switching mechanism in HOIP-based RS devices. It's also worth noting that a rather high ON/OFF ($>10^9$) ratio was observed in quasi-2D halide perovskite-based devices with excellent endurance by Kim *et al.*[20,21], which implies the huge potential commercial applications of HOIP-based RS memories.

In this work, $MAPbBr_3$ single crystal was chose for the conduction study, because $MAPbBr_3$ is non-polar (centrosymmetric)[22] and therefore ferroelectricity could be excluded, while the influence of grain boundaries can also be ignored. Compared with polycrystalline thin films, $MAPbX_3$ single crystals present lower trap density and much better environmental stability, which can be considered as an ideal platform for investigating their intrinsic physical properties. The electric-field-driven resistance switching accompany by a diode-like behavior was produced in the Au/$MAPbBr_3$/Au structure. The diode-like switchable effect can be explained by the formation of reversible p-n junctions induced by ion immigration in the crystals. The area-proportional conduction indicates an interface-type RS behavior, which is related to the charge trapping/detrapping process at the interface.

■ EXPERIMENTAL SECTION

The $MAPbBr_3$ single crystals were prepared from solution by inverse temperature crystallization (ITC) method.[23] The raw materials methylammonium bromide (CH_3NH_3Br, 99.5%), lead bromide ($PbBr_2$, 99.9%), N, N-dimethylformamide (DMF, 99%), and dimethylsulfoxide (DMSO, 99%) were used as received. CH_3NH_3Br and $PbBr_2$ with a molar

ratio of 1:1 were dissolved in DMSO-DMF (7:3 by volume) to form a solution, and $MAPbBr_3$ was crystallized at the temperature from 60 °C to 100 °C with a heating rate of 0.2 - 0.5 °C/h.

An X-ray diffractometer (XRD, PANalytical X'pert) was used for phase identification at room temperature. The absorption spectra were measured in the wavelength range of 400–800 nm using an UV spectrometer (SpectraPro-275, Acton Research Corporation). Au (100 nm) was used as the electrode for electrical characteristics. The top-electrode has two different sizes with 6×6 mm^2 and 6×3 mm^2, while the bottom electrode has a size of 6×7 mm^2. The current-voltage (*I-V*) measurements were carried out using a semiconductor analyzer (FS380, Platform Design Automation, Inc.) assisted with a probe station (Lakeshore TTPX). To avoid the influence of the environmental gases and moisture,[24] the samples were kept in a vacuum chamber for electrical characteristics with a pressure of 10^{-4} mbar.

■ RESULTS AND DISCUSSION

The inset of Figure 1a shows an optical image of an $MAPbBr_3$ single crystal with dimensions of ~ 6×7×2 mm^3. Figure 1a presents the typical XRD 2θ scan data of the $MAPbBr_3$ single crystal at room temperature. The crystal adopts a pure cubic phase with good crystallization and high quality, which could be further confirmed by the surface and cross-section SEM images (Figure S1). The element mapping results (Figure S2) reveal that the partitioning and segregation of Br or Pb are absent in the crystals. The absorbance of $MAPbBr_3$ (Figure 1b) shows a clear band edge cutoff at 568 nm with no excitonic signature, matching the values of the band edge cutoff and the photoluminescence peak position reported earlier for the same single crystals grown using ITC process.[23] The optical band gap of $MAPbBr_3$ could be

determined to be 2.17 eV by extrapolating the linear region of the absorption edge to the energy-axis intercept, which is similar to the other reports.[22]

Figure 2 shows the dark current of the Au/$MAPbBr_3$/Au structure with different scanning rates and directions in two different scale. The arrows in the figure depict the bias scanning directions. The sequence of voltage sweep is $0 \rightarrow +80$ V $\rightarrow 0 \rightarrow -80$ V $\rightarrow 0$, where the voltage is termed as positive when the top electrode is positively biased. A clear switchable diode-like RS behavior is observed in Figure 2, which is quite different from the previous work on HOIP thin film devices.[9-16] In most of these films, only resistive switching but no diode-like behavior was mentioned. The diode direction can be switched during the sweep process in the dark. During the scan path 2, the device switches to the LRS. When the scan direction reverses in the path 3 the current abruptly decrease and the device switches to HRS. The on/off ratio of the dark current is ~ 54 at a bias of +10 V. Figure S3 displays the *I-V* curves of an Au/$MAPbBr_3$/Au device in the dark with different measurement voltages. It is interesting to find that the switchable diode-like RS is observed even under a low voltage at 1 V. The *I-V* curves show clearly variation in the "set" voltages without an evident electroforming process.

We now focus on the possible origin of the switchable diode-like resistive switching. The switchable diode-like RS generally occurs in ferroelectric devices,[25] where the barrier height at the ferro/electrode interface could be controlled by the switchable ferroelectric polarization. Actually, the switchable diode behavior has been observed in Au/$MAPbI_3$/ITO thin film devices, which results in a giant switchable photovoltaic effect under illumination.[26] According to the proposed mechanism in refs. 26 and 27, since $MAPbBr_3$ is a non-ferroelectric, the switchable diode can be understood in terms of the defects electromigration process, as shown in Figure 3. It is known that many types of point defects have been reported in the HOIPs, such as V_{Pb}'', $V_{Br}^{\bullet}$,

V'_{MA}, etc. Positively-charged Br vacancy ($V^{\bullet}_{Br}$) can lead to n-type doping, whereas negatively charged Pb and MA vacancies (V''_{Pb} and V'_{MA}) result in p-type doping.[28] Provided that the defects are mobile charges, they can move through the sample under electric fields to find a new thermodynamic equilibrium. For instance, V'_{MA} can move and pile up near the bottom surface for negative bias conditions. Thus, the top surface region acquires n-type carriers, whereas the region near the bottom electrode becomes p-type. Yuan *et al.* have reported a direct observation of MA^+ ion and V'_{MA} migration under a bias field.[29] The reversible inner p-i-n structure induced by ion drift has also been confirmed directly in $MAPbI_3$ thin films.[26]

The rectifying current-voltage traces (path 2→3 and 4→1) are attributed to the p-n junction created through the asymmetric distribution of charged defects, which is also believed to induce of a RS behavior directly. The low resistance state (LRS) can be attributed to the creation of p-n junction. By applying an opposite electric field, the inhomogeneous donor/or acceptor distribution can be reversed to an evenly distributed insulating state (HRS). For a full sweep cycle (Figure 2), scan path 1 (HRS) is quite sensitive to the scanning rate, which just reveals the defects electromigration process. Path 1 displays the forming process of the p-n structure from an evenly defect distribution. After the creation of inner p-n junction, the Au/$MAPbBr_3$/Au structure shows a low resistance state and its current is then not sensitive to scan speed (path 2 in Figure 2). The I-V traces of path 3 and 4 show strongly scan speed-dependent because it corresponds to the establishment of a reverse p-n junction (point C, D, E in Figure 3), where the defects electromigration process is time- and voltage-dependent.

Although the defects electromigration approach can be used to describe the switchable diode-like resistive switching in $MAPbBr_3$ single crystal-based devices, the detailed charge transport mechanism is still unclear. In the previous reports on HOIP-based RS devices, the

switching operations were attributed to the creation and annihilation of conducting filaments.[11-13] However, the filamentary conduction and the inner p-n junction cannot coexist. Furthermore, the filamentary scenario cannot explain the asymmetrical and electrode-area dependent *I-V* results. Figure 4 displays the RS behavior of an Au/$MAPbBr_3$/Au device with different sizes of top-electrode. It can be seen that both the HRS and LRS are electrode area-dependent, which could be regarded as a rejection of an filamentary-type resistive switching.[30] Furthermore, as shown in Figure 2, the hysteresis loops in one sweep cycle obtained under forward and reverse biases are asymmetrical, which further excludes the interface-type RS nature. These asymmetrical loops can be observed more conspicuously in a Pt/$MAPbBr_3$/Pt device (see Figure 6a).

The most common RS process related to electronic mechanisms include: Schottky barrier modulation, tunneling at the interface, hopping conduction, and charge trapping/detrapping at the interface or in the bulk.[9,30] It was previously reported that Au and Pt form an Ohmic contact with HOIPs.[10,31] Then the interfacial Schottky barrier[10,16] scenario should be excluded in our case. To further understand the conduction mechanism, we replotted the *I-V* curves of HRS in a log-log scale as shown in Figure 4. Two regions were evident in the HRS curves. At low voltages, the *I-V* response was ohmic ($I \infty V$). At high fields, the current exhibited a rapid non-linear rise and signaled the transition onto the trap-filled limit (TFL) regime, in which all the available trap states were filled by the injected carriers.[32] The *I-V* response of the trap-filled SCLC is marked by a steep increase in current ($I \infty V^{n>3}$). The onset voltage V_{TFL} (V_{TFL} =37 *V* for Pt electrodes and 39 *V* for Au electrodes) is typically linearly proportional to the density of trap states as follows,[22]

$$V_{TFL} = 8en_t d^2/9\varepsilon\varepsilon_0 \qquad (1)$$

Where n_t is the density of trap states, d is the thickness of the sample, ε is the dielectric constant (here we use 25 for $MAPbBr_3$), and ε_0 is the vacuum permittivity. Correspondingly, it could be found that our $MAPbBr_3$ single crystals have a medium trap density of ~1.5×10^{12} cm^{-3}.

According to the above results, it is concluded that the main conduction mechanism in our device should be the trap-controlled SCLC by the charged defects. Besides the inner p-n junction, the empty traps can also lead to a high resistance state, while if all the traps are filled, the injected carriers can move freely into the perovskite crystals and then lead to a low resistance state. The next question is the charge trapping/detrapping at the interface or in the bulk? Figure S4 displays the contact resistance and bulk resistance of the Au/$MAPbBr_3$/Au devices. The calculation results indicate that the contact resistance between the Au electrode and the crystal is about 10 Ω, which is much smaller than the bulk resistance (~10^8 Ω). This suggests that the resistive switching occurs through bulk trap generation, moving and filling in the $MAPbBr_3$.

Interestingly, the trap moving and filling states can be modulated by light absorption. Figure 6a, b, and c show the *I-V* curves of a Pt/$MAPbBr_3$/Pt device in the dark, under light illumination and subsequent light off, respectively. For the initial measurement in the dark, the switching loop under reverse bias is severely restricted, which implies a weakened resistive switching. This means the p-n junction was not established and the traps were not fully filled in this sweep process. The speculation could be confirmed by further SCLC analysis as shown in Figure 6d. The characteristic I-V traces in the initial dark state showing only a linear ohmic regime ($I \propto V$). After light illumination, some of the traps/defects are "activated" and then could be filled by injected carriers (Figure 6d). Figure 8 illustrates the evolution of RS behavior of Au/$MAPbBr_3$/Au device under light illumination with different intensity. Under the light illumination, both the HRS and LRS currents increase due to the existence of photocurrent. The

resistive switching loops became narrower than the dark case, and wore off eventually. The results of light-responsive experiments also exclude the possible of metallic filaments mechanism for the observed RS behavior.

It should be mentioned that the recent results from Hong et al.[17] have shown that the switchable diode-like RS behavior can be induced solely by an interface charge trapping/-detrapping mechanism. Two back-to-back diodes could be formed due to the change in the interfacial barrier width (Figure S5). However, the interface resistance is much smaller than the bulk one in our devices, and the series conduction is governed by the bulk state. It is worth noting that the trap-controlled SCLC could be used to describe not only the conduction of an charge trapping/detrapping process, but also the defects electromigration process.[26,33] The aforementioned switchable diode-like RS behavior can be then explained by the formation of an electric-field-driven p-n junction accompanied by a trap-controlled SCLC in the perovskite. The resistance state (HRS and LRS) depends on the synergy between the inner p-n junction and the charge trapping/detrapping states.

■ CONCLUSIONS

In summary, a switchable diode-like RS behavior was observed in $MAPbBr_3$ single crystals using Au (or Pt) symmetric electrodes. The dependence of the trap generation, moving and filling states play a vital role on the resistance switching. The charged defects migrate under applying a bias and lead to a reversible p-n structure in the crystal. The rectifying current-voltage traces and the LRS are attributed to the p-n junction created through the asymmetric distribution of charged defects. The inhomogeneous charged trap distribution can be reversed to an evenly distributed insulating state (HRS) by an opposite electric field. Accompanying, charge

trapping/detrapping occurs associate with the mobile traps. The resistive switching behavior is then further enhanced by this trap-controlled SCLC conduction process.

■ ASSOCIATED CONTENT

■ AUTHOR INFORMATION

Corresponding Author

*E-mail: wl@ncu.edu.cn (L.W.)

*E-mail: llshu@ncu.edu.cn (L.S.)

Author Contributions

S.K. and L.S. conceived the idea, designed the experiments and interpreted the results. J.G., S.L. and L.Q. performed the $MAPbBr_3$ single crystal fabrications. J.Z., R.L., and Y.Z. carried out the XRD, electrical and optical measurements. B.L. and B.C. discussed the resistive switching mechanism. S.K., L.W. and L.S. prepared the paper. All authors discussed the results and have given approval to the final version of the manuscript.

Notes

The authors declare no competing financial interest.

■ ACKNOWLEDGMENTS

This work was supported by the National Natural Science Foundation of China (Nos. 11964017, 51972157, 11864022 and 51662028), and the Natural Science Foundation of Jiangxi Province (No. 20192ACB21017).

■ REFERENCES

[1] Huang, C.; Lin, P.; Fu, N.; Liu, C.; Xu, B.; Sun, K.; Wang, D.; Zeng, X.; Ke, S. Facile fabrication of highly efficient ETL-free perovskite solar cells with 20% efficiency by defect passivation and interface engineering. *Chem. Commun.* **2019,** *55*, 2777-2780.

[2] Kim H, Han JS, Choi J, Kim SY, Jang HW. Halide perovskites for applications beyond photovoltaics. *Small Methods* 2018, **2**: 1700310.

[3] Kim H, Huynh KA, Kim SY, Le QV, Jang HW. 2D and quasi-2D halide perovskites: applications and progress. *Phys. Stat. Solid. RRL* 2020, **14**: 1900435.

[4] Zhu, H.; Fu, Y.; Meng, F.; Wu, X.; Gong, Z.; Ding, Q.; Gustafsson, M. V.; Trinh, M. T.; Jin, S.; Zhu, X. Y. Lead halide perovskite nanowire lasers with low lasing thresholds and high quality factors. *Nat. Mater.* **2015,** *14*, 636-642.

[5] Long, M.; Zhang, T.; Chai, Y.; Ng, C.-F.; Mak, T. C. W.; Xu, J.; Yan, K. Nonstoichiometric acid–base reaction as reliable synthetic route to highly stable $CH_3NH_3PbI_3$ perovskite film. *Nat. Commun.* **2016,** *7*, 13503.

[6] Rakita, Y.; Bar-Elli, O.; Meirzadeh, E.; Kaslasi, H.; Peleg, Y.; Hodes, G.; Lubomirsky, I.; Oron, D.; Ehre, D.; Cahen, D. Tetragonal $CH_3NH_3PbI_3$ is ferroelectric. *Proc. Natl. Acad. Sci.* **2017,** *114*, E5504-E5512.

[7] Snaith, H. J.; Abate, A.; Ball, J. M.; Eperon, G. E.; Leijtens, T.; Noel, N. K.; Stranks, S. D.; Wang, J. T.-W.; Wojciechowski, K.; Zhang, W. Anomalous Hysteresis in Perovskite Solar Cells. *J. Phys. Chem. Lett.* **2014,** *5*, 1511-1515.

[8] Azpiroz, J. M.; Mosconi, E.; Bisquert, J.; De Angelis, F. Defect migration in methylammonium lead iodide and its role in perovskite solar cell operation. *Energy Environ. Sci.* **2015,** *8*, 2118-2127.

[9] Yoo, E. J.; Lyu, M.; Yun, J.-H.; Kang, C. J.; Choi, Y. J.; Wang, L. Resistive Switching Behavior in Organic–Inorganic Hybrid $CH_3NH_3PbI_{3-x}Cl_x$ Perovskite for Resistive Random Access Memory Devices. *Adv. Mater.* **2015,** *27*, 6170-6175.

[10] Guan, X.; Hu, W.; Haque, M. A.; Wei, N.; Liu, Z.; Chen, A.; Wu, T. Light-Responsive Ion-Redistribution-Induced Resistive Switching in Hybrid Perovskite Schottky Junctions. *Adv. Funct. Mater.* **2018,** *28*, 1704665.

[11] Gu, C.; Lee, J.-S. Flexible Hybrid Organic–Inorganic Perovskite Memory. *ACS Nano* **2016,** *10*, 5413-5418.

[12] Choi, J.; Park, S.; Lee, J.; Hong, K.; Kim, D.-H.; Moon, C. W.; Park, G. D.; Suh, J.; Hwang, J.; Kim, S. Y.; Jung, H. S.; Park, N.-G.; Han, S.; Nam, K. T.; Jang, H. W. Organolead Halide Perovskites for Low Operating Voltage Multilevel Resistive Switching. *Adv. Mater.* **2016,** *28*, 6562-6567.

[13] Hwang, B.; Lee, J.-S. A Strategy to Design High-Density Nanoscale Devices utilizing Vapor Deposition of Metal Halide Perovskite Materials. *Adv. Mater.* **2017,** *29*, 1701048.

[14] Choi, J.; Le, Q. V.; Hong, K.; Moon, C. W.; Han, J. S.; Kwon, K. C.; Cha, P.-R.; Kwon, Y.; Kim, S. Y.; Jang, H. W. Enhanced Endurance Organolead Halide Perovskite Resistive Switching Memories Operable under an Extremely Low Bending Radius. *ACS Appl. Mater. Interfaces* **2017,** *9*, 30764-30771.

[15] Yoo, E.; Lyu, M.; Yun, J.-H.; Kang, C.; Choi, Y.; Wang, L. Bifunctional resistive switching behavior in an organolead halide perovskite based Ag/$CH_3NH_3PbI_{3-x}Cl_x$/FTO structure. *J. Mater. Chem. C* **2016,** *4*, 7824-7830.

[16] Zhou, F.; Liu, Y.; Shen, X.; Wang, M.; Yuan, F.; Chai, Y. Low-Voltage, Optoelectronic $CH_3NH_3PbI_{3-x}Cl_x$ Memory with Integrated Sensing and Logic Operations. *Adv. Funct. Mater.* **2018,** *28*, 1800080.

[17] Tian J, Wu H, Fan Z, *et al.* Nanoscale topotactic phase transformation in $SrFeO_x$ epitaxial thin films for high-density resistive switching memory. *Adv. Mater.* 2019, **31**: 1903679.

[18] Kim H, Han JS, Kim SG, Kim SY, Jang HW. Halide perovskites for resistive random-access memories. *J. Mater. Chem. C* 2019, **7**: 5226-5234.

[19] Hong, Z.; Zhao, J.; Li, S.; Cheng, B.; Xiao, Y.; Lei, S. Tunable hysteresis behaviour related to trap filling dependence of surface barrier in an individual $CH_3NH_3PbI_3$ micro/nanowire. *Nanoscale* **2019,** *11*, 3360-3369.

[20] Kim H, Choi MJ, Suh JM, Han JS, Kim SG, Le QV, Kim SY, Jang HW. Quasi-2D halide perovskites for resistive switching devices with ON/OFF ratios above 10^9. *NPG Asia Mater.* 2020, **12**: 21.

[21] Lee S, Kim H, Kim DH, et al. Tailored 2D/3D halide perovskite heterointerface for substantially enhanced endurance in conducting bridge resistive switching memory. *ACS Appl. Mater. Interfaces* 2020, **12**: 17039-17045.

[22] Shi, D.; Adinolfi, V.; Comin, R.; Yuan, M.; Alarousu, E.; Buin, A.; Chen, Y.; Hoogland, S.; Rothenberger, A.; Katsiev, K. Low trap-state density and long carrier diffusion in organolead trihalide perovskite single crystals. *Science* **2015,** *347*, 519-522.

[23] Liu, Y.; Yang, Z.; Cui, D.; Ren, X.; Sun, J.; Liu, X.; Zhang, J.; Wei, Q.; Fan, H.; Yu, F.; Zhang, X.; Zhao, C.; Liu, S. Two-Inch-Sized Perovskite $CH_3NH_3PbX_3$ (X = Cl, Br, I) Crystals: Growth and Characterization. *Adv. Mater.* **2015,** *27*, 5176-5183.

[24] Fang, H.-H.; Adjokatse, S.; Wei, H.; Yang, J.; Blake, G. R.; Huang, J.; Even, J.; Loi, M. A. Ultrahigh sensitivity of methylammonium lead tribromide perovskite single crystals to environmental gases. *Sci. adv.* **2016,** *2*, e1600534.

[25] Tian, J.; Tan, Z.; Fan, Z.; Zheng, D.; Wang, Y.; Chen, Z.; Sun, F.; Chen, D.; Qin, M.; Zeng, M. Depolarization-Field-Induced Retention Loss in Ferroelectric Diodes. *Phys. Rev. Appl.* **2019,** *11*, 024058.

[26] Xiao, Z.; Yuan, Y.; Shao, Y.; Wang, Q.; Dong, Q.; Bi, C.; Sharma, P.; Gruverman, A.; Huang, J. Giant switchable photovoltaic effect in organometal trihalide perovskite devices. *Nat. Mater.* **2015,** *14*, 193-198.

[27] Lampert, M. A.; Mark, P. Current injection in solids. *New York, NY : Academic Press* **1970**.

[28] Game, O. S.; Buchsbaum, G. J.; Zhou, Y.; Padture, N. P.; Kingon, A. I. Ions Matter: Description of the Anomalous Electronic Behavior in Methylammonium Lead Halide Perovskite Devices. *Adv. Funct. Mater.* **2017,** *27*, 1606584.

[29] Yuan, Y.; Chae, J.; Shao, Y.; Wang, Q.; Xiao, Z.; Centrone, A.; Huang, J. Photovoltaic Switching Mechanism in Lateral Structure Hybrid Perovskite Solar Cells. *Adv. Energy. Mater.* **2015,** *5*, 1500615.

[30] Bagdzevicius, S.; Maas, K.; Boudard, M.; Burriel, M. Interface-type resistive switching in perovskite materials. *J. Electroceram.* **2017,** *39*, 157-184.

[31] Saidaminov, M. I.; Adinolfi, V.; Comin, R.; Abdelhady, A. L.; Peng, W.; Dursun, I.; Yuan, M.; Hoogland, S.; Sargent, E. H.; Bakr, O. M. Planar-integrated single-crystalline perovskite photodetectors. *Nat. Commun.* **2015,** *6*, 8724.

[32] Lian, Z.; Yan, Q.; Gao, T.; Ding, J.; Lv, Q.; Ning, C.; Li, Q.; Sun, J.-l. Perovskite $CH_3NH_3PbI_3(Cl)$ Single Crystals: Rapid Solution Growth, Unparalleled Crystalline Quality, and Low Trap Density toward 10^8 cm^{-3}. *J. Am. Chem. Soc.* **2016,** *138*, 9409-9412.

[33] Xiong Z.; Hu W.; She Y.; Lin Q.; Hu L.; Tang X.; Sun K. Air-stable lead-free perovskite thin film based on $CsBi_3I_{10}$ and its application in resistive switching devices. *ACS Appl. Mater. Interfaces* **2019,** *11*, 30037-30044.

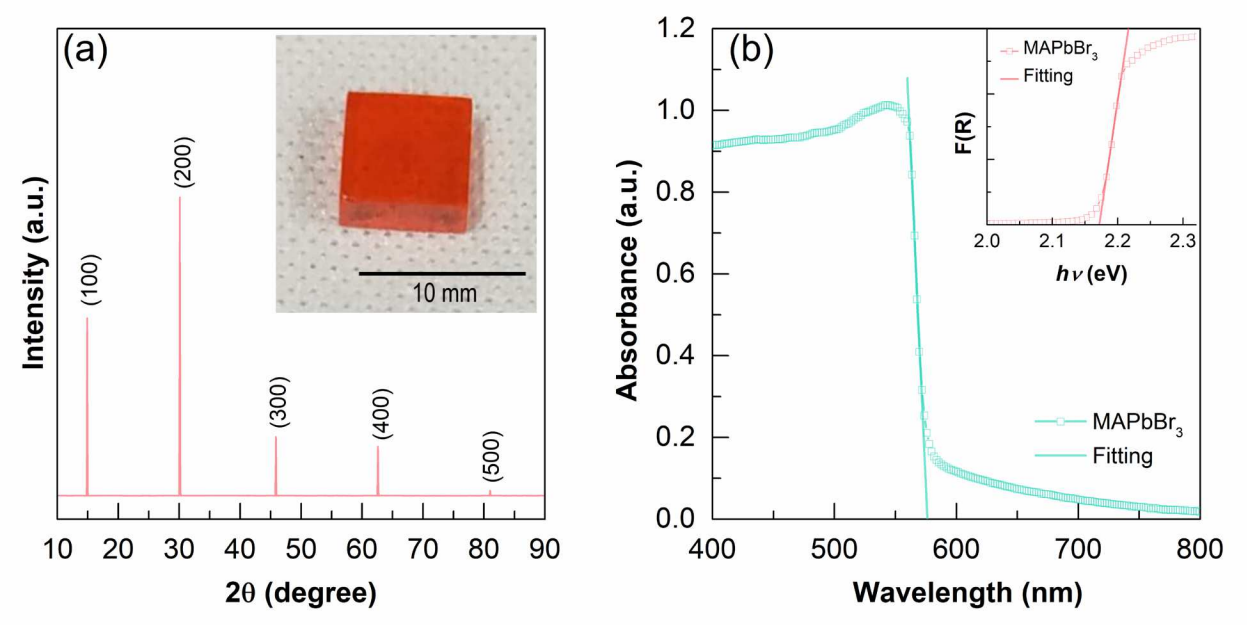

Figure 1. (a) XRD and (b) absorption spectra of $MAPbBr_3$ single crystals. Inset: (a) image of one of the measured crystals grown from solution; (b) absorbance versus photon energy and the determined band gap E_g.

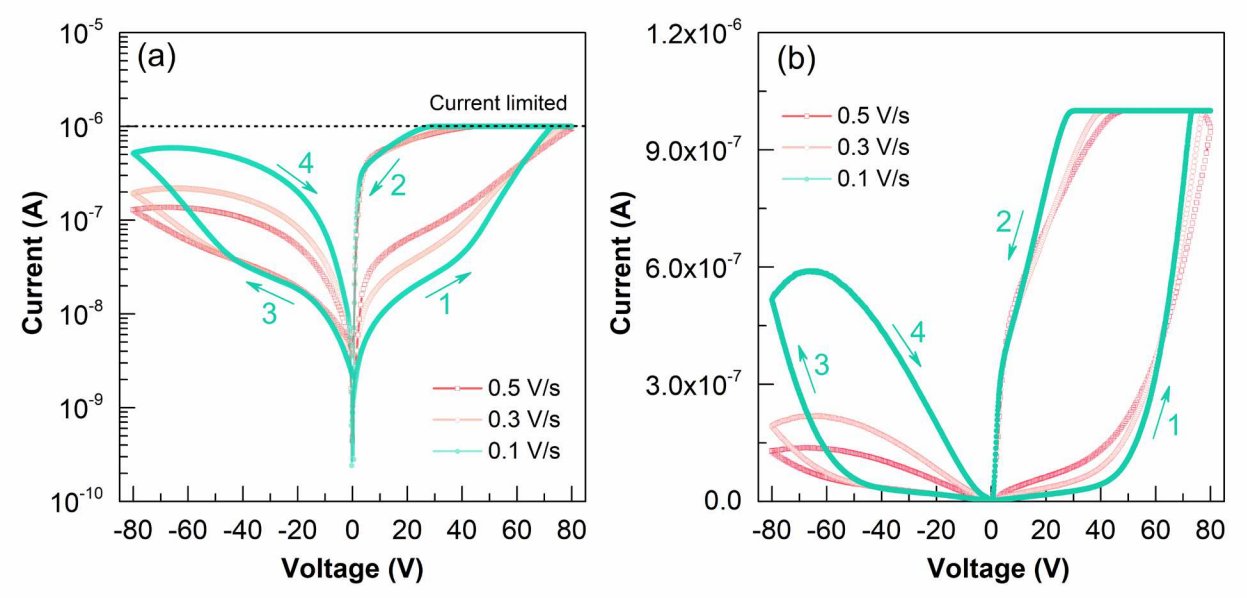

Figure 2. Current-voltage traces. *I-V* curves of an Au/$MAPbBr_3$/Au device in (a) log-scale and (b) normal-scale in the dark with different scanning rates. All the measurements were conducted at room temperature in a vacuum chamber.

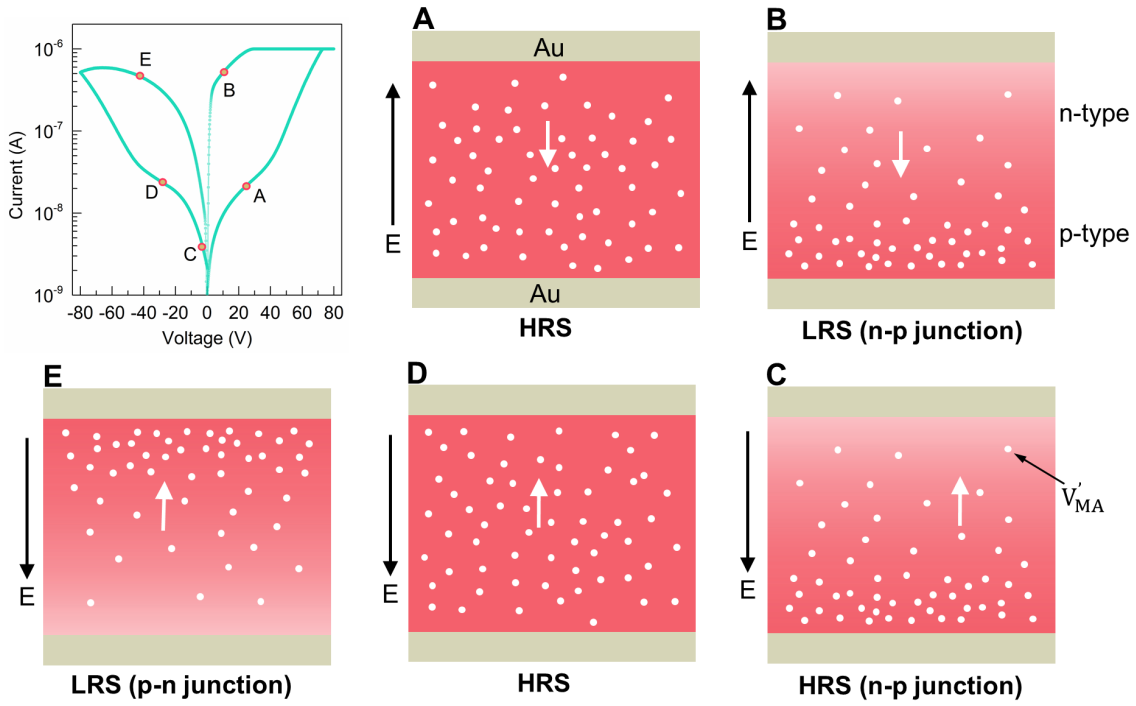

Figure 3. Schematic diagram describing the rectifying and resistive switching behavior of electronic states in $MAPbBr_3$ single crystal. Negatively charged V'_{MA} is focused here, and the inclusion of other defects actually does not alter the conclusion. The MA vacancies respond to electric field. In a negative field (bottom to up), MA vacancies are moving downward and accumulating near the bottom surface and are frozen when the field is turned off. As a result, a state with p-type carriers is realized; the opposite region becomes a n-type conductor.

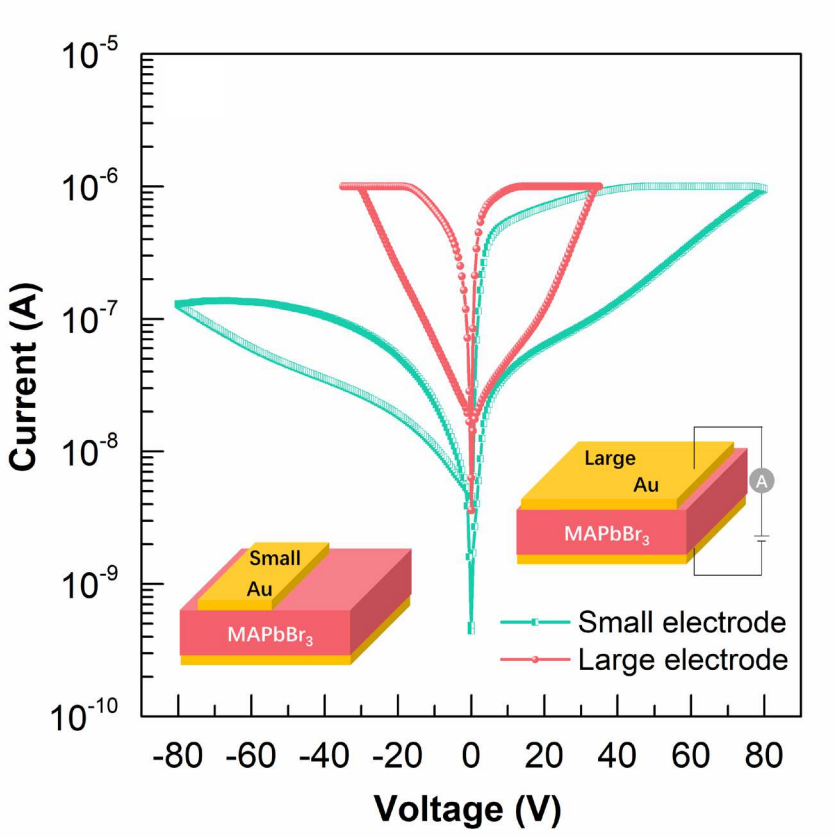

Figure 4. *I-V* curves of an Au/$MAPbBr_3$/Au device in the dark with different top-electrode area.

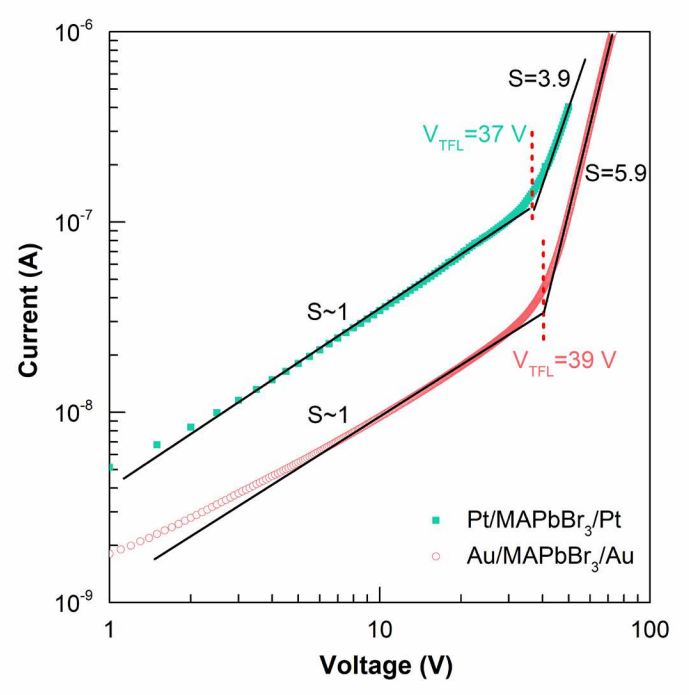

Figure 5. The high resistance state of $MAPbBr_3$ single crystals with Au and Pt electrodes in a log-log scale. Characteristic *I-V* traces showing two different regimes. A linear ohmic regime ($I \infty V$) is followed by the trap-filled regime ($I \infty V^{n>3}$).

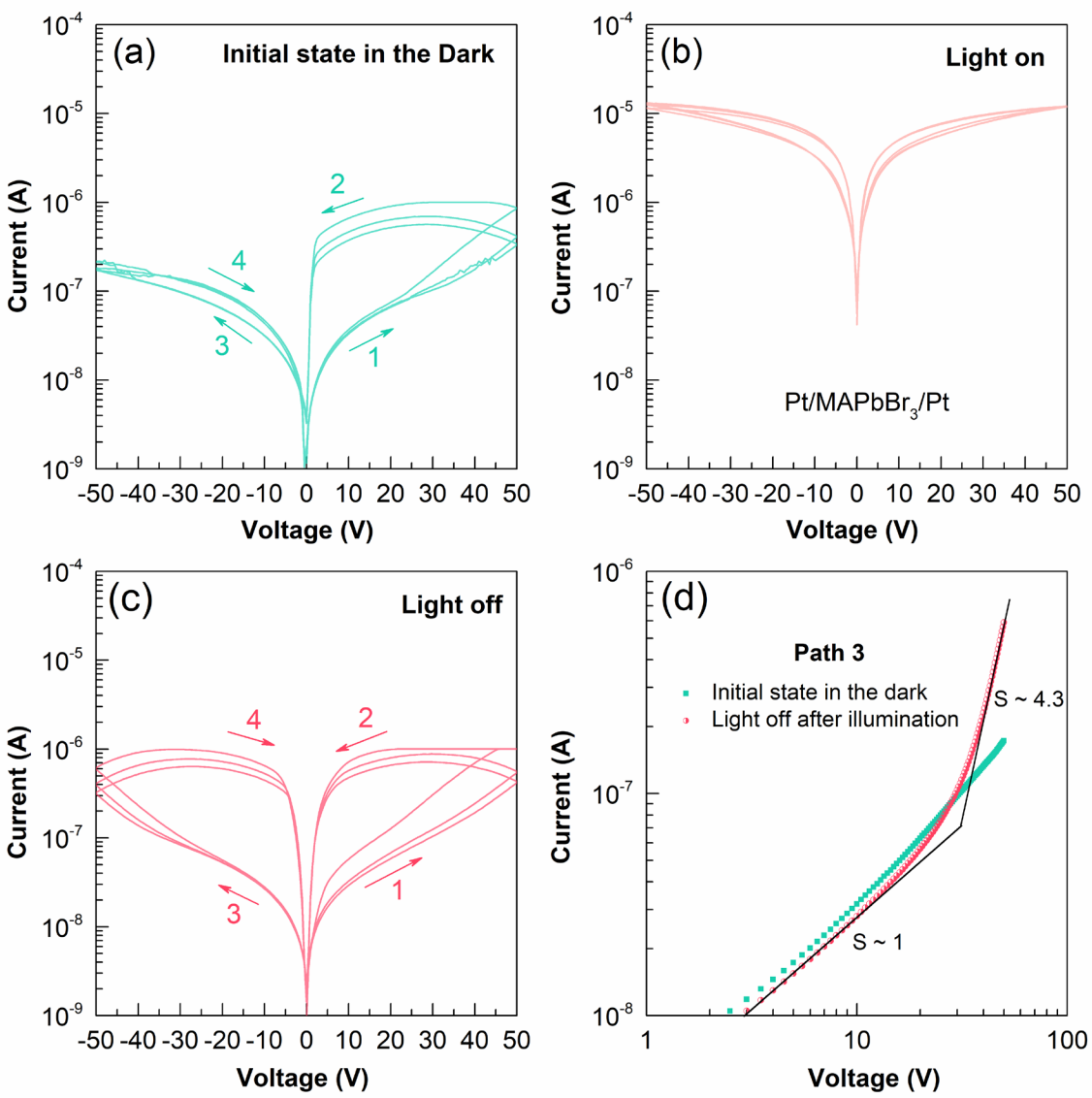

Figure 6. *I-V* curves of a Pt/MAPbBr3/Pt device (a) in the dark, (b) under light illumination (1500 LUX) and (c) subsequent light off. (d) The so-called high resistance state (path 3 under reverse bias) of $MAPbBr_3$ single crystals with Pt electrodes in a log-log scale. Characteristic *I-V* traces in the initial dark state showing only a linear ohmic regime ($I \propto V$), while a trap-filled regime ($I \propto V^{n>3}$) could be found after light illumination.

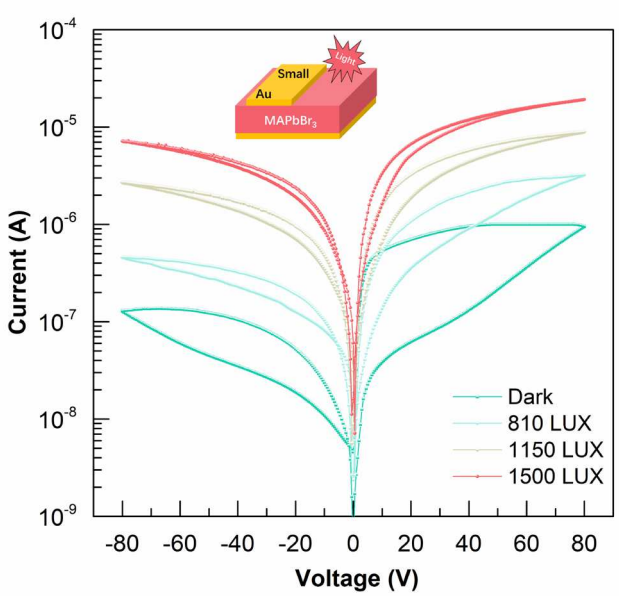

Figure 7. *I-V* curves of an Au/$MAPbBr_3$/Au device under light illumination with selected power density.

Figures

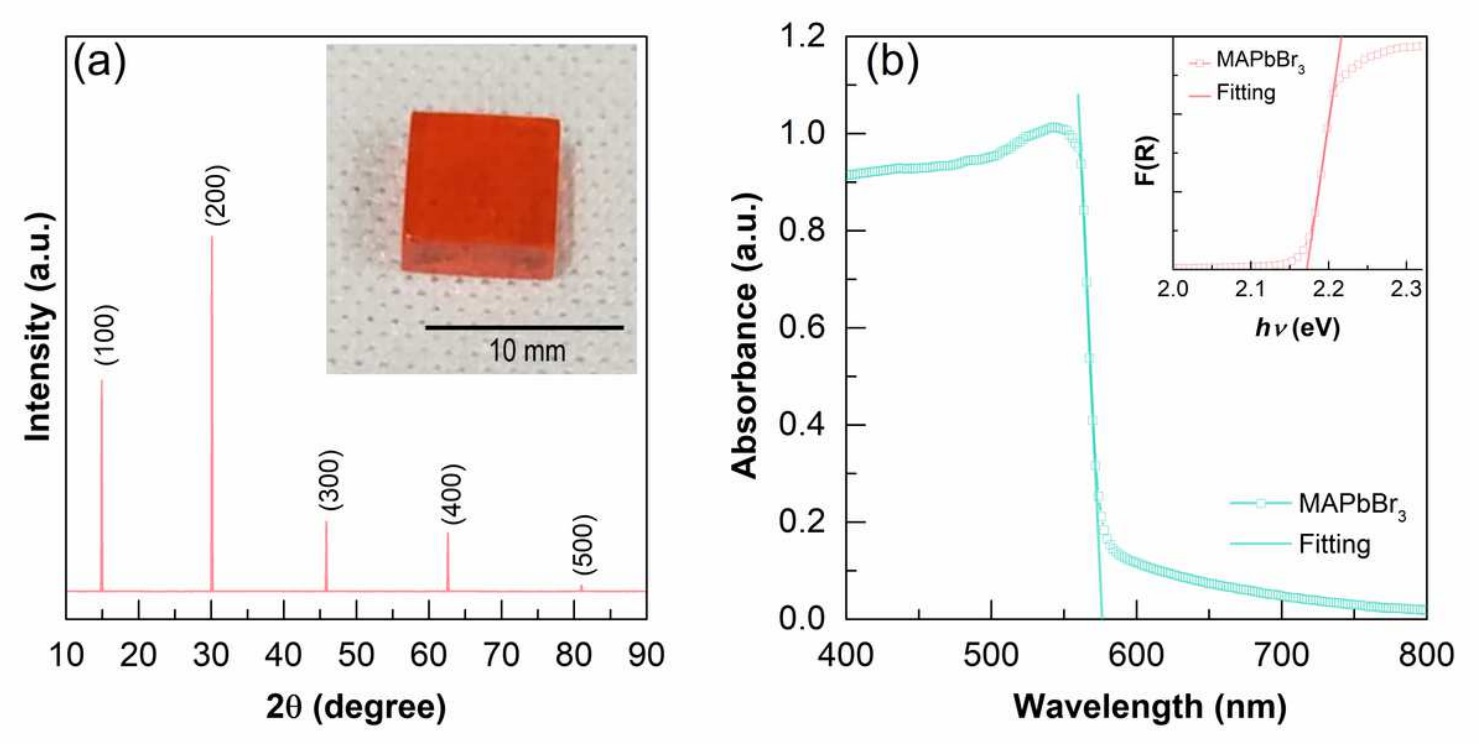

Figure 1

(a) XRD and (b) absorption spectra of MAPbBr3 single crystals. Inset: (a) image of one of the measured crystals grown from solution; (b) absorbance versus photon energy and the determined band gap Eg.

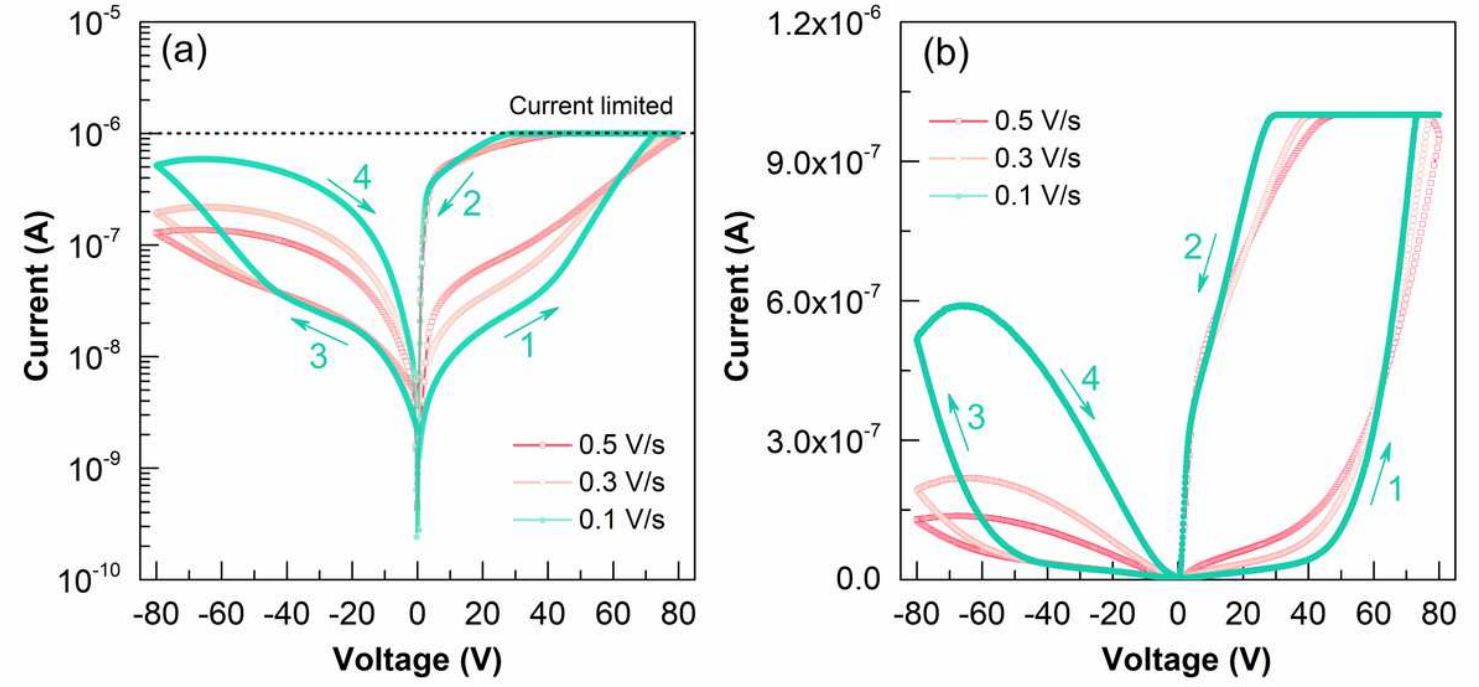

Figure 2

Current-voltage traces. I-V curves of an Au/MAPbBr3/Au device in (a) log-scale and (b) normal-scale in the dark with different scanning rates. All the measurements were conducted at room temperature in a vacuum chamber.

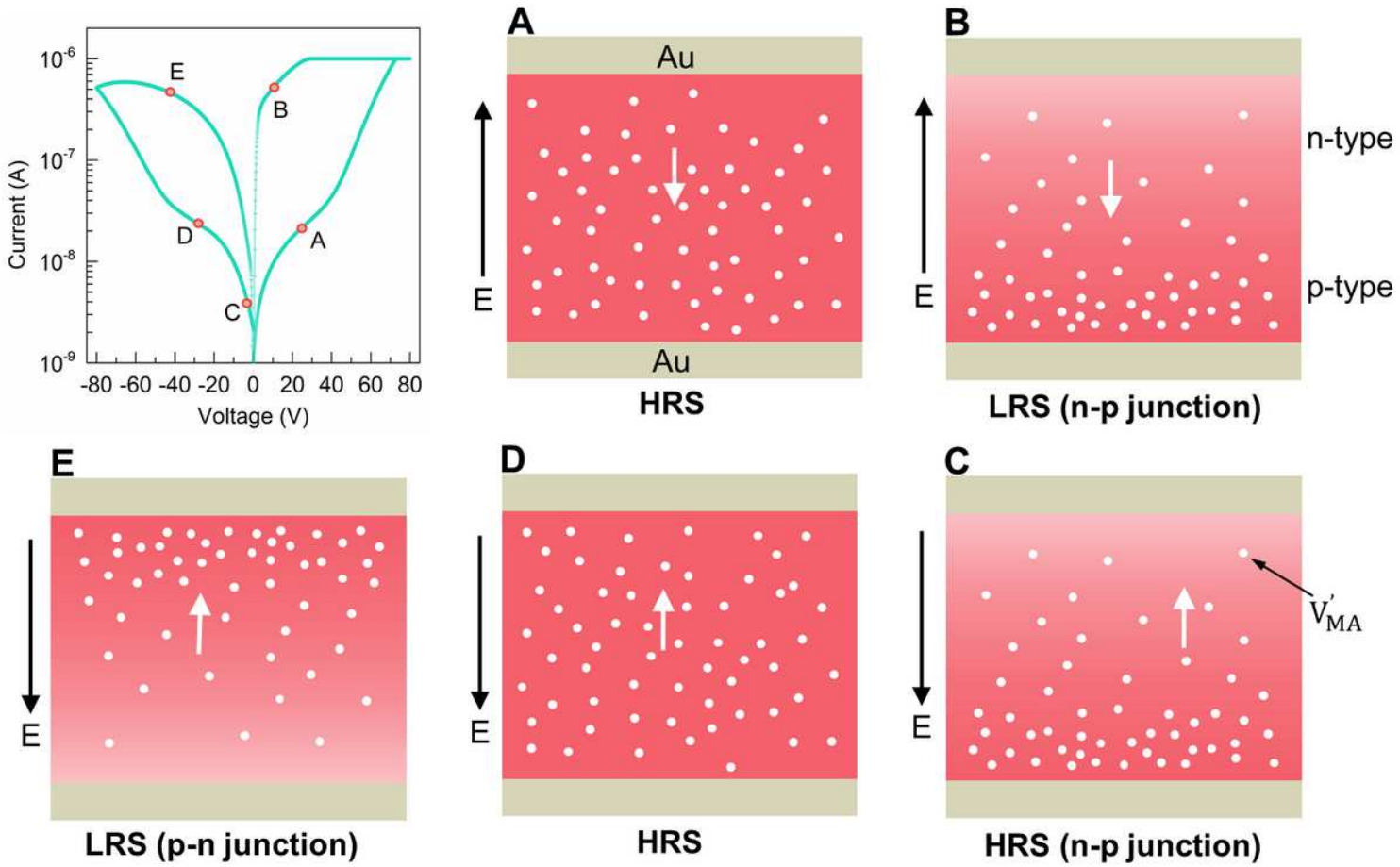

Figure 3

Schematic diagram describing the rectifying and resistive switching behavior of electronic states in MAPbBr3 single crystal. Negatively charged V'MA is focused here, and the inclusion of other defects actually does not alter the conclusion. The MA vacancies respond to electric field. In a negative field (bottom to up), MA vacancies are moving downward and accumulating near the bottom surface and are frozen when the field is turned off. As a result, a state with p-type carriers is realized; the opposite region becomes a n-type conductor.

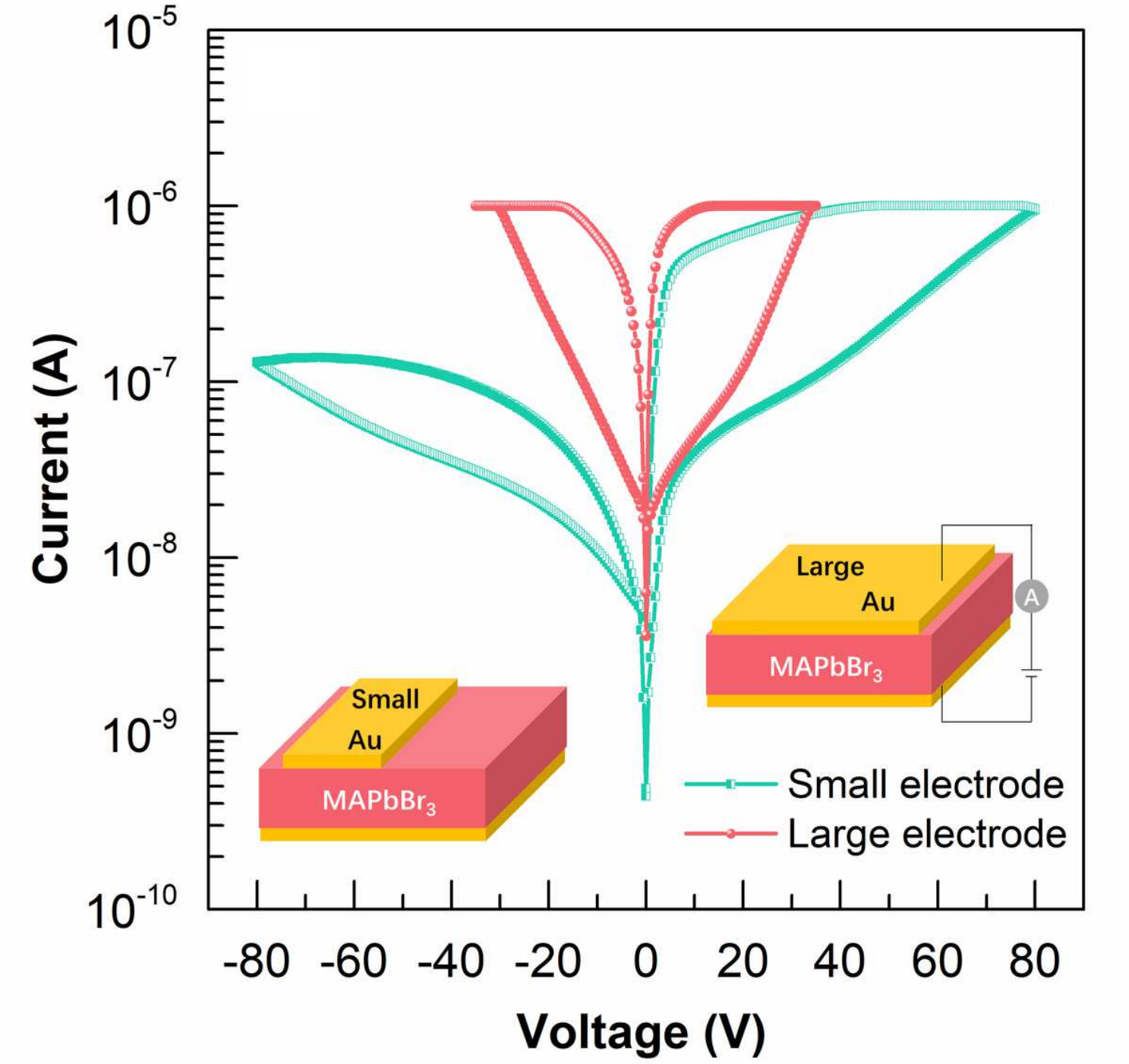

Figure 4

I-V curves of an Au/MAPbBr3/Au device in the dark with different top-electrode area.

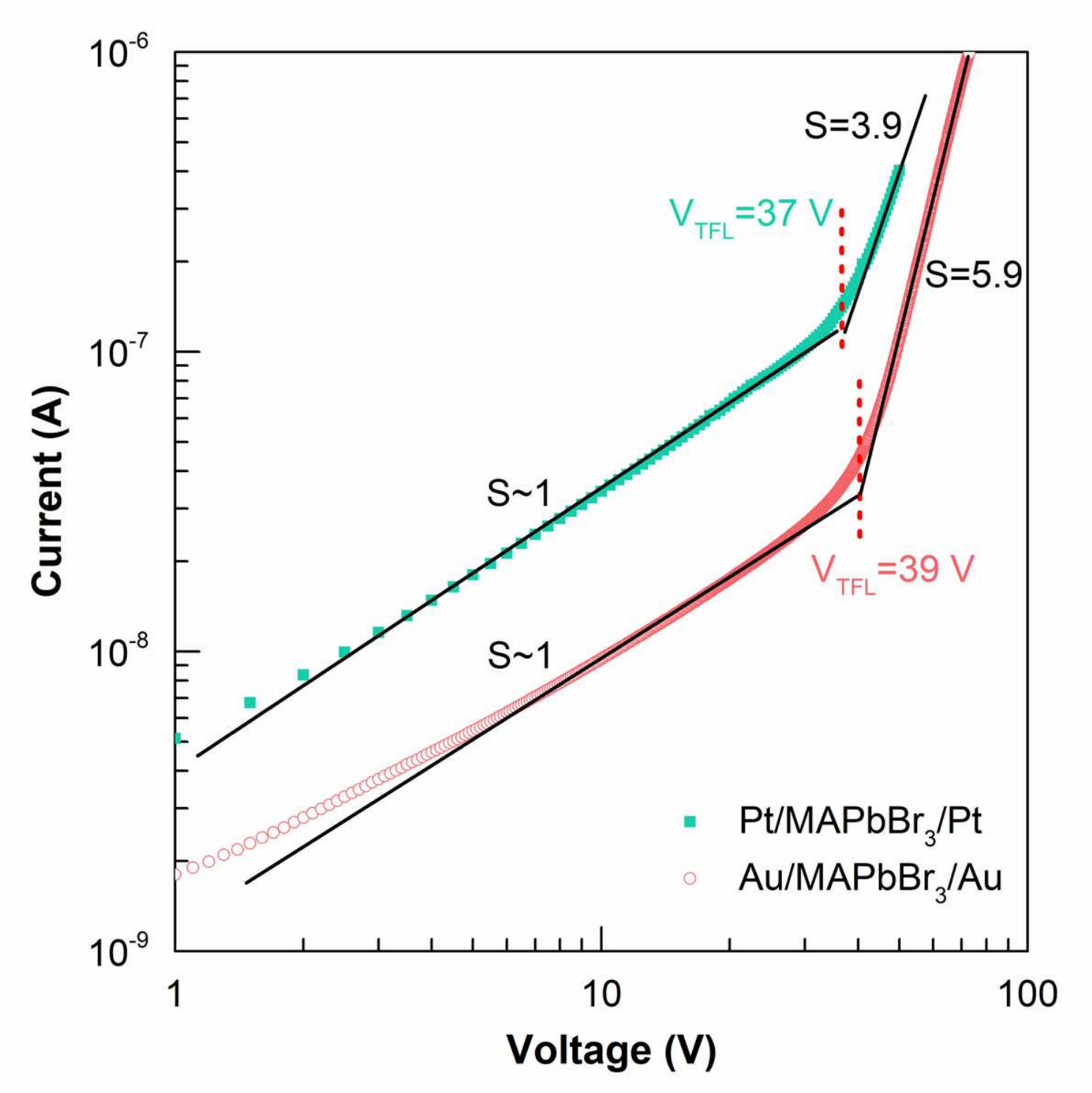

Figure 5

The high resistance state of MAPbBr3 single crystals with Au and Pt electrodes in a log-log scale. Characteristic I-V traces showing two different regimes. A linear ohmic regime (I ∞ V) is followed by the trap-filled regime (I ∞ Vn>3).

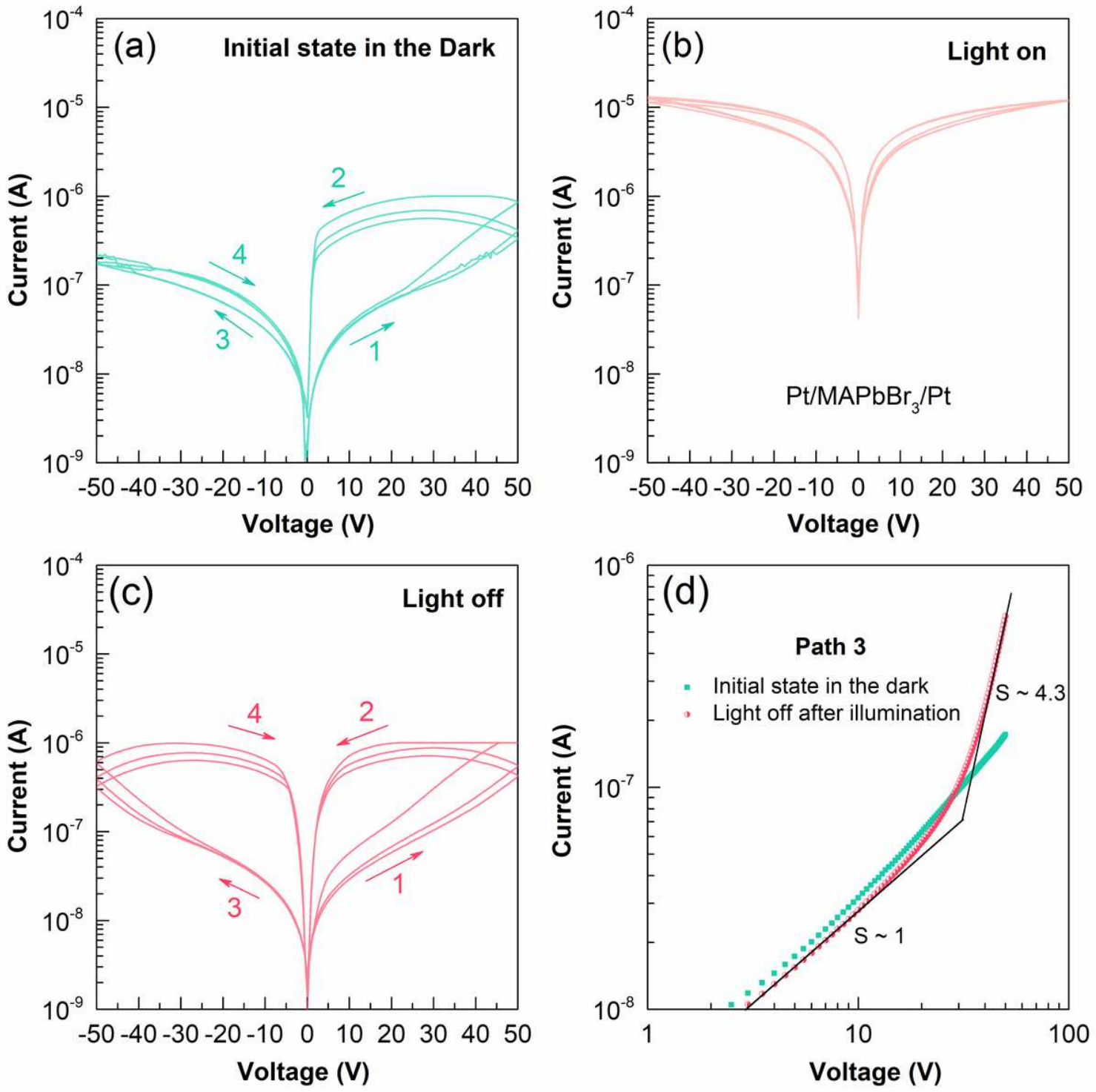

Figure 6

I-V curves of a Pt/MAPbBr3/Pt device (a) in the dark, (b) under light illumination (1500 LUX) and (c) subsequent light off. (d) The so-called high resistance state (path 3 under reverse bias) of MAPbBr3 single crystals with Pt electrodes in a log-log scale. Characteristic I-V traces in the initial dark state showing only a linear ohmic regime ($I \propto V$), while a trap-filled regime ($I \propto V^{n>3}$) could be found after light illumination.

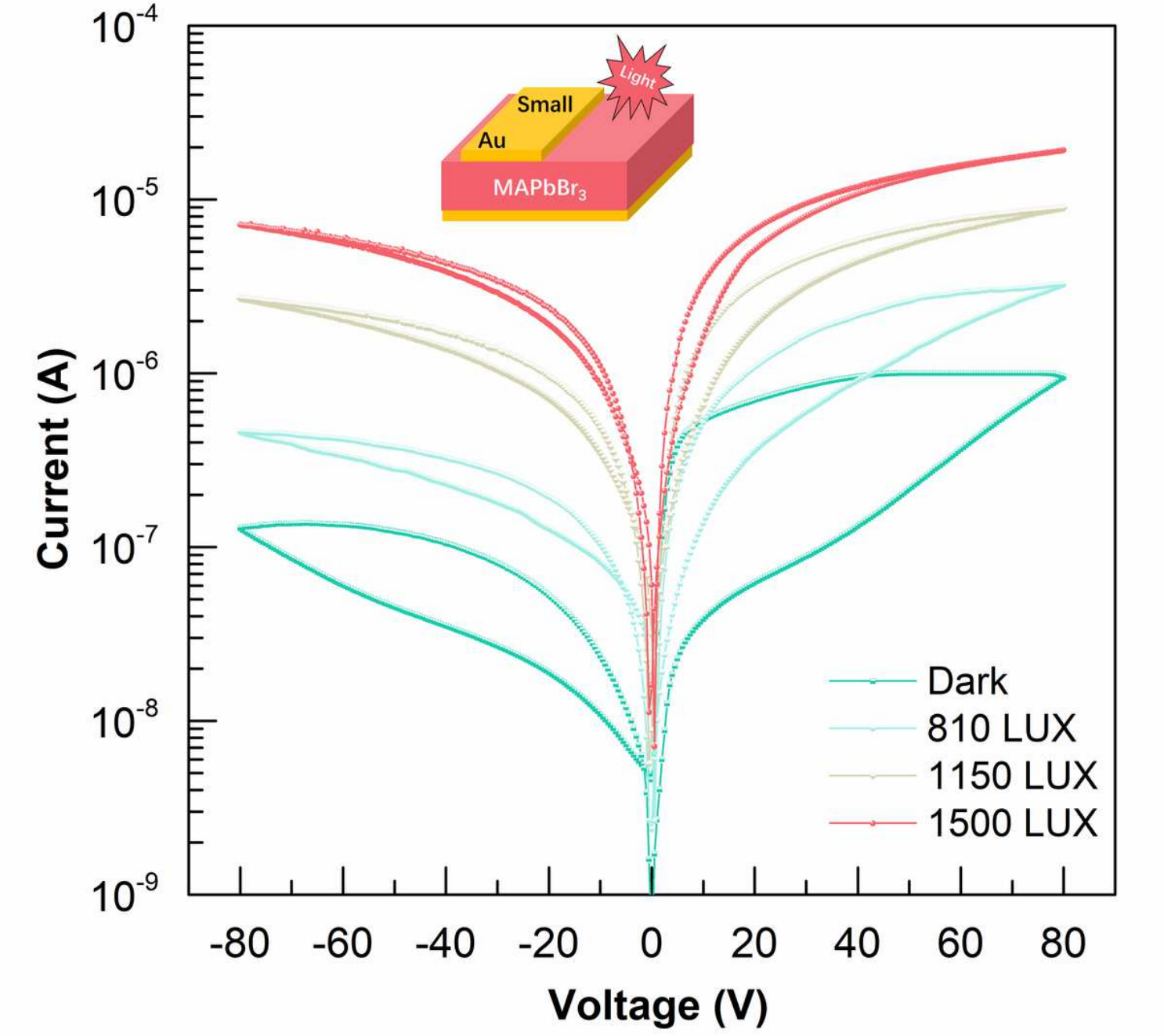

Figure 7

I-V curves of an Au/MAPbBr3/Au device under light illumination with selected power density.